Hybrid adaptive chassis control for vehicle lateral stability in the presence of uncertainty

Dhruv Jagga, Maolong Lv, and Simone Baldi

Abstract— To guarantee the safety of passengers in a wide range of driving situations, vehicle lateral stability should be achieved in the presence of nonlinear dynamics (consequence of critical maneuvers) and uncertainty (consequence of uncertain parameters). This paper designs a hybrid adaptive strategy to attain vehicle stability in these situations. The design is based on a piecewise affine (PWA) description of the vehicle model where partitions describe both the linear and the nonlinear regimes, and where parametric uncertainties are handled by estimators for the control gains that can adapt to different conditions acting on the system. Comparisons with strategies that merely exploits the linear region of the vehicle dynamics are provided for different driving conditions, and performance improvements of the proposed methodology are assessed.

Keywords: Integrated chassis control, PWA vehicle model, Hybrid adaptive control.

I. INTRODUCTION

Safety is one of the objectives of automotive research [1]: to achieve this goal, a crucial role is played by the ability to control the vehicle dynamics over a wide range of situations, including handling nonlinear behavior and uncertain conditions. Normal driving conditions cover only the linear handling regime, but critical maneuvers bring the vehicle in nonlinear handling regimes. At this point safety should be guaranteed by driver assistance systems like Anti-lock Braking Systems (ABS), Electronic Stability Program (ESP), or Active Front Steering (AFS) [2]. However, there are many reported examples when driver assistance systems are not able to effectively handle nonlinear regimes, especially in the presence of parametric uncertainty [3].

Several chassis control algorithms have been proposed of which a non-exhaustive overview is given. A combination of linear feedback and feedforward control has been used in [4] to govern the yaw rate and sideslip angle. Linear quadratic regulation (LQR) and H_∞ were used in [5]. Insufficient performance of linear control during nonlinear regimes has stimulated the application of nonlinear algorithms [6]: techniques such as neural network [10], [11], fuzzy logic [12] and rule-based control [13] have been applied to chassis control. The use of a PWA system to model the nonlinearities has been proposed in [7], [8], and state feedback PWA design was used in [9] to coordinate the steering and distribution of torque. However, no uncertainty has been considered in these works. Using a PWA vehicle model is recognized as a pragmatic way to control the nonlinear system at different

The authors are with Delft Center for Systems and Control, Delft University of Technology, The Netherlands. email: jaggadhruv@gmail.com, {m.lyu,s.baldi}@tudelft.nl

operating points defined by a set of linear subsystems: each subsystem approximates the nonlinear vehicle in the vicinity of operating points which cover the operating range of interest. The transitions between subsystems are modeled as "switches": this gives rise to the so-called hybrid control paradigm where the controller has to guarantee stability in the presence of such transitions. Only in recent years efforts have been made towards adaptive control strategies for these hybrid systems [14], [15], [16], [17], [18], [19], to effectively handle uncertainty. This work stems from this line of research, and aims at verifying the applicability of these techniques to chassis control: in fact, chassis control coping with both linear and nonlinear handling regimes remains an open problem which motivates the research in this paper. Our hybrid adaptive control design is based on a PWA description of the vehicle model, where partitions describe both the linear and nonlinear regimes, and where parametric uncertainties are handled by estimators for the control gains that can adapt to different conditions acting on the system.

II. VEHICLE MODELING

The bicycle model is the most widely used 2-DOF vehicle model which can capture the essential lateral steering and yaw dynamics [20], [21], [22]. The lateral dynamics of the vehicle are derived via the equations of motion

$$
\begin{aligned}
mv_x(\dot{\beta} + r) &= 2F_f cos(\delta_f) + 2F_r \\
I_z \dot{r} &= 2l_f F_f cos(\delta_f) - 2l_r F_r + \Delta M
\end{aligned}
\tag{1}
$$

where β is the side slip angle of the vehicle and r is the yaw rate, F_f and F_r are the lateral forces acting on the front and rear lumped tires, l_f and l_r are the distances of the center of gravity of the vehicle from the front and rear axle, m is the mass of the vehicle, I_z is yaw inertia, δ_f is steering angle of front tire and ΔM is corrective yaw moment which is the result of differential braking. For small side slip angles for the front and rear tires, the following holds:

$$
\alpha_f = \delta_f - (\beta + \frac{l_f r}{v_x}), \quad \alpha_r = -(\beta - \frac{l_r r}{v_x}).
\tag{2}
$$

The Pacejka's tire model, also known as Magic Formula, is used to describe the non-linearities in the tire characteristics [23]. In the disjoint case, with the lateral force with pure slip, the tire forces can be expressed by

$$
\begin{aligned}
F_f &= D_f \sin(C_f \operatorname{atan}(B_f \alpha_f - E_f(B_f \alpha_f - \operatorname{atan}(B_f \alpha_f))) \\
F_r &= D_r \sin(C_r \operatorname{atan}(B_r \alpha_r - E_r(B_r \alpha_r - \operatorname{atan}(B_r \alpha_r)))
\end{aligned}
\tag{3}
$$
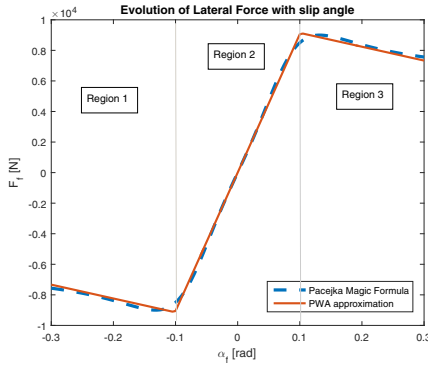
Fig. 1: Pacejka magic formula for front tire force and PWA approximation according to partitioning of tire sideslip angle. The figure has been derived for under-steering behavior (cf. Table III).

A. Piecewise-affine (PWA) vehicle model

The 2-DOF vehicle model in (1) is nonlinear: in order to make it amenable for control, we provide a PWA approximation of it. This can be done by partitioning of the nonlinear lateral tire forces into polyhedral sets [6]. Lateral tire forces acting on the front tire are given by

$$F_f(\alpha_f) = \begin{cases} d_f \alpha_f - e_f & , \text{if } -\hat{\alpha}_f < \alpha_f \\ c_f \alpha_f & , \text{if } -\hat{\alpha}_f < \alpha_f < \hat{\alpha}_f \\ d_f \alpha_f + e_f & , \text{if } \alpha_f > \hat{\alpha}_f \end{cases} \quad (4)$$

where d_f and e_f are used to approximate the front tire forces in the corresponding partition with straight lines. The partitions depends upon the slip angle α_f. This is most clearly seen in the three partitions in Figure 1: from the picture it is clear that region 2 corresponds to the linear handling regime, while regions 1 and 3 to nonlinear handling regimes. Rear tire forces $F_r(\alpha_r)$ are assumed to be linear[1]

$$F_r(\alpha_r) = c_r \alpha_r. \quad (5)$$

At this point, the nonlinear system represented by (1) can be linearized around uniform rectilinear motion (i.e. for v_x = constant, $\beta = 0$, $r = 0$, $\delta_f = 0$). As a consequence, the vehicle dynamics can be represented as a PWA system:

$$\dot{x} = A_i x + B_i u + f_i, \qquad i = \{1, 2, 3\} \quad (6)$$

where i is the index indicating the partition, $x = \begin{bmatrix} \beta & r \end{bmatrix}^T$ is the state, $u = \begin{bmatrix} \delta_f & \Delta M \end{bmatrix}^T$ is the input comprising front steering angle and the differential yaw moment, and

$$A_i = \begin{pmatrix} -\frac{2d_{fi} + 2d_{ri}}{mv_x} & -1 - 2\frac{d_{fi}l_f - 2d_{ri}l_r}{mv_x^2} \\ -2\frac{d_{fi}l_f - 2d_{ri}l_r}{I_z} & -2\frac{d_{fi}l_f^2 + 2d_{ri}l_r^2}{I_z v_x} \end{pmatrix}$$

$$B_i = \begin{pmatrix} 2\frac{d_{fi}}{mv_x} & 0 \\ 2\frac{d_{fi}l_{fi}}{I_z} & \frac{1}{I_z} \end{pmatrix} \qquad f_i = \begin{pmatrix} \mp 2\frac{e_{fi} + e_{ri}}{mv_x} \\ \mp 2\frac{e_{fi}l_{fi} - e_r l_r}{I_z} \end{pmatrix}. \quad (7)$$

[1]For easiness of exposition, only the nonlinear characteristics of the front tire are taken into account: considering nonlinear rear tire forces is possible but would lead to more partitions that make plots more difficult to interpret.

The partitions of the PWA system (6) can be described in terms of α_f. In fact, the active partition depends upon the front tire slip angle as described through the approximation of tire force function (4) (if one considers nonlinear rear tire forces, one would obtain partitions depending on both α_f and α_r). The switching among partitions, activated by appropriate guard conditions, is represented through the hybrid automaton of Figure 2, with β_0 and r_0 being the initial states of the system. The combination of (6), (7) and the switching of Figure 2 leads to a time-varying (switched) system described as

$$\dot{x} = A(t)x(t) + B(t)u(t) + f(t) \quad (8)$$

$$A(t) = \sum_{i=1}^{3} A_i \chi_i(t), \ B(t) = \sum_{i=1}^{3} B_i \chi_i(t), \ f(t) = \sum_{i=1}^{3} f_i \chi_i(t) \quad (9)$$

where $A(t)$, $B(t)$, $f(t)$ take different values at different time instants as specified by the set (A_i, B_i, f_i). To describe switching, the indicator function χ_i is used, similarly to [24].

III. HYBRID ADAPTIVE CONTROL POLICY

In practice, the matrices in (7) contain uncertain parameters, requiring a control action that can cope with uncertainty and switched dynamics. The subsequent control design relies on the hybrid adaptive approach of [24], with some ad-hoc modifications for the system at hand.

A. Hybrid reference model

A reference model is specified individually for each partition of the PWA system, as follows

$$\dot{x}_{mi} = A_{mi}x_{mi} + B_{mi}r + f_{mi} \quad (10)$$

where $r = \begin{bmatrix} \beta_d & r_d \end{bmatrix}^T \in \mathbb{R}^2$ is reference signal, and the matrices $A_{mi} \in \mathbb{R}^{2 \times 2}$, $B_{mi} \in \mathbb{R}^{2 \times 2}$, $i \in I$, were chosen with A_{mi} Hurwitz. Here, x_m is a continuous reference trajectory which has to be followed by x. The stability properties of the reference model can be derived via the Lyapunov equation:
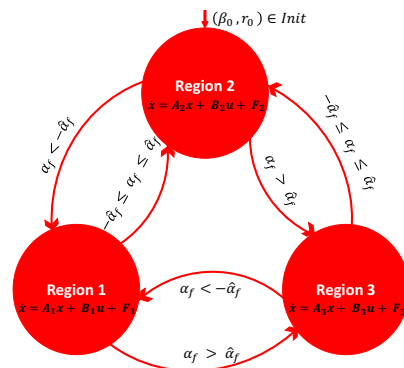
$$A_{mi}^T P_{mi} + P_{mi}A_{mi} = -Q_{mi} \quad (11)$$

Fig. 2: Switching between subsystems depending upon the evolution of front tire slip angle (α_f)
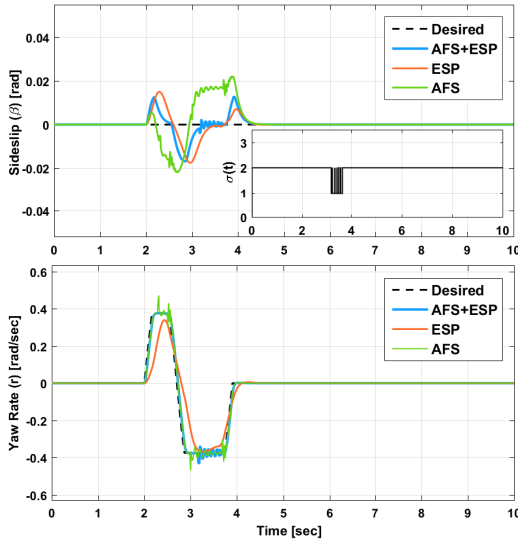
Fig. 3: Closed-loop response with vehicle velocity of $20m/s$ in SWD maneuver with hybrid adaptive control (in the small plot the switching signal is shown).

Fig. 4: Closed-loop response with vehicle velocity of $20m/s$ in SWD maneuver with linear controller.

where $P_{mi}, Q_{mi} \in \mathbb{R}^{2\times 2}$ are symmetric and positive definite. Since in our simulations we were always able to find a common Lyapunov matrix P_m such that $A_{mi}^T P_m + P_m A_{mi} < 0$, in the following we will concentrate on the common Lyapunov matrix case [26], [27], [28].

B. Adaptive control design

A state feedback adaptive control exists provided that certain assumptions are met [29].

Assumption 1: There exist constant matrices $K_i^* \in \mathbb{R}^{2\times 2}$, invertible constant matrices $L_i^* \in \mathbb{R}^{2\times 2}$ and constant vectors $M_i^* \in \mathbb{R}^2$, such that

$$
\begin{aligned}
A_{mi} &= A_i + B_i K_i^{*T} \\
B_{mi} &= B_i L_i^* \\
f_{mi} &= f_i + B_i M_i^* = 0.
\end{aligned}
\tag{12}
$$

Assumption 2: There exists known matrices $S_i \in \mathbb{R}^{2\times 2}$, such that $G_i = L_i^* S_i$ are symmetric and positive definite.

1) Controller structure and error model: If the vehicle parameters were perfectly known, the nominal control law to achieve the closed loop stability of the system would be

$$
u(t) = K^{*T}(t)x(t) + L^*(t)r(t) + M^*(t)
\tag{13}
$$

$$
K^*(t) = \sum_{i=1}^{3} K_i^* \chi_i(t), \; L^*(t) = \sum_{i=1}^{3} L_i^* \chi_i(t), \; M^*(t) = \sum_{i=1}^{3} M_i^* \chi_i(t)
\tag{14}
$$

However, as the ideal gains in (12) are unknown in view of the unknown matrices A_i and B_i, we need to employ some estimates in the control action, that is
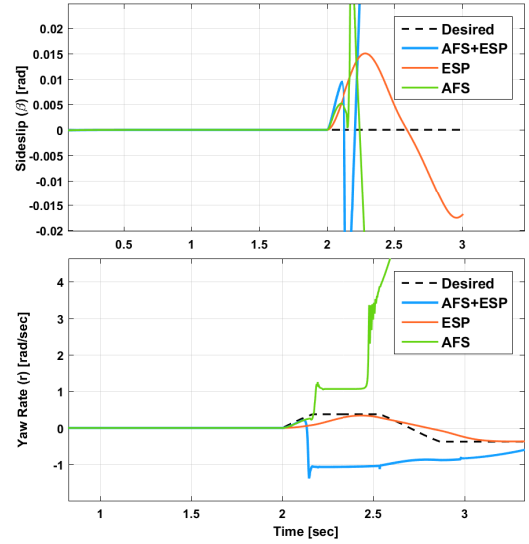
$$
u(t) = K^T(t)x(t) + L(t)r(t) + M(t)
\tag{15}
$$

$$
K(t) = \sum_{i=1}^{3} K_i(t)\chi_i(t), \; L(t) = \sum_{i=1}^{3} L_i(t)\chi_i(t), \; M(t) = \sum_{i=1}^{3} M_i(t)\chi_i(t)
\tag{16}
$$

and K_i, L_i, M_i are the estimates of K_i^*, L_i^*, M_i^* respectively.

The dynamics (8), (10) and the controller (15) lead to the dynamics of the state tracking error $e = x - x_m$

$$
\dot{e} = \dot{x} - \dot{x}_m = \sum_{i=1}^{3}(A_{mi}\chi_i e + B_{mi}L_i^{*-1}\chi_i(\tilde{K_i}^T x + \tilde{L}_i r + \tilde{M}_i))
\tag{17}
$$

where $\tilde{K_i}^T(t) = K_i^T(t) - K_i^{*T}$, $\tilde{L}_i(t) = L_i(t) - L_i^*$ and $\tilde{M}_i(t) = M_i(t) - M_i^*$, $i \in I$ are the parametric estimation errors. With some modifications to the approach in [24] in order to account for the constant term in (15), it is possible to derive the following adaptive laws

$$
\begin{aligned}
\dot{K_i^T}(t) &= -S_i^T B_{mi}^T \chi_i(t) P_m e(t) x^T(t) \\
\dot{L_i}(t) &= -S_i^T B_{mi}^T \chi_i(t) P_m e(t) r^T(t) \\
\dot{M_i}(t) &= -S_i^T B_{mi}^T \chi_i(t) P_m e(t)
\end{aligned}
\tag{18}
$$

where P_m is the common Lyapunov matrix. The following result holds:

Theorem 3.1 ([24]): In the presence of a common Lyapunov matrix P_m, the state tracking error converges asymptotically to zero for arbitrarily fast switching.

Proof: See [24] with minor modifications. ∎

Remark 3.1: Any adaptive mechanism is strongly affected by the presence of unmodelled dynamics, cf. [24], [16], [25]. In the following section we address this topic from a simulation point of view, where unmodelled dynamics appear due to variation of longitudinal speed and due to a nonlinear rear tire that is included in the simulations, but not in the control design.
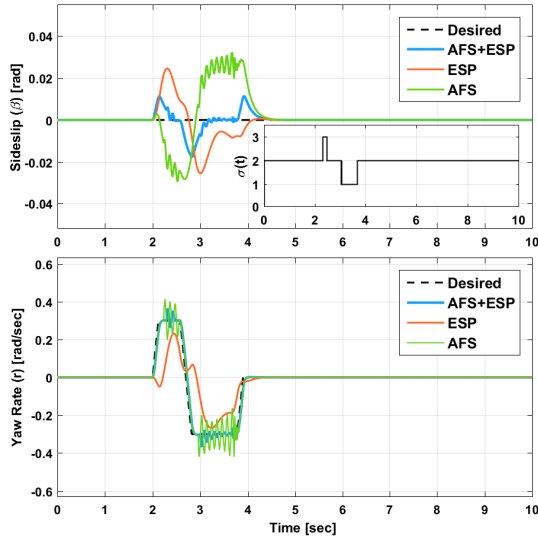
Fig. 5: Closed-loop response with vehicle velocity of $25m/s$ in SWD maneuver with hybrid adaptive control (in the small plot the switching signal is shown).

Fig. 6: Closed-loop response with vehicle velocity of $25m/s$ in SWD maneuver with linear controller.

IV. SIMULATION RESULTS

This section is devoted to assess the performance of the hybrid adaptive controller. All the parameters of the vehicle model under consideration can be found in the tables in Appendix. The controller was designed at standard test vehicle velocity of $20\ m/s$. The first step is the design of the stable reference model to determine the desired behavior of the vehicle. Using a similar approach to [24], the reference model (10) has been designed via linear quadratic controller (LQ) of the form of $u^* = K_i^{*T}x(t) + L_i^*r(t) + M_i^*$ where the gains are based on some nominal knowledge of the matrices (A_i, B_i, f_i). The state feedback gains K_i^* were chosen by using linear quadratic state feedback regulator with $Q_1 = Q_3 = 100\ I_2$, $Q_2 = 10\ I_2$ and $R_i = 10\ I_2$. We obtain,

$$K_1^*, K_3^* = \begin{bmatrix} -6.2596 & -1.5358 \\ 2.59 \cdot 10^{-4} & 1.01 \cdot 10^{-4} \end{bmatrix},$$

$$K_2^* = \begin{bmatrix} 0.4785 & 0.6370 \\ 2.36 \cdot 10^{-6} & 4.64 \cdot 10^{-6} \end{bmatrix}.$$

The feedforward gains were taken as $L_i^* = -(C_i A_{mi}^{-1} B_i)^{-1}$, such that the diagonal elements of the transfer matrix $\Gamma(s) = C_i(sI - A_{mi})^{-1}B_i L_i^*$ have DC gain equal to one, that is

$$L_1^*, L_3^* = \begin{bmatrix} -23.4846 & -4.3341 \\ -4.78 \cdot 10^5 & -2.13 \cdot 10^4 \end{bmatrix},$$

$$L_2^* = \begin{bmatrix} 3.3010 & 0.9976 \\ -4.78 \cdot 10^5 & -2.13 \cdot 10^4 \end{bmatrix}.$$

Finally, the gains M_i^* were chosen to achieve equilibrium in the origin for every partition, that is

$$M_1^*, M_3^* = \begin{bmatrix} -1.1094 \\ 0 \end{bmatrix}, \qquad M_2^* = \begin{bmatrix} 0 \\ 0 \end{bmatrix}.$$
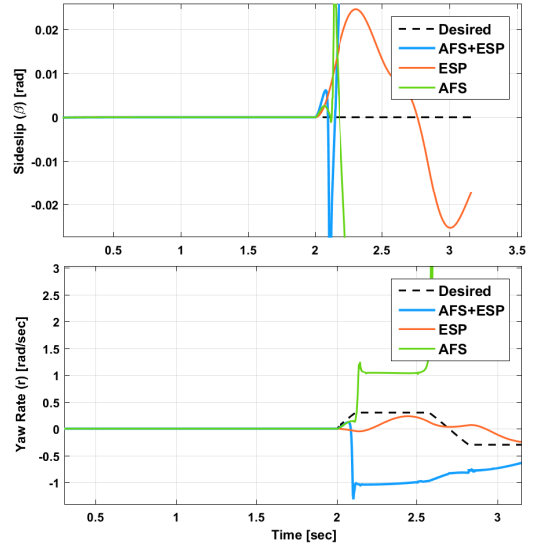
A common Lyapunov matrix was found to be:

$$P_m = \begin{bmatrix} 7.1950 & -0.3469 \\ -0.3469 & 1.0194 \end{bmatrix}$$

The effectiveness of the controller was exhibited by using various tests with Sine with Dwell steering (SWD, this kind of steering allows to excite the nonlinear vehicle regimes). The simulations, both for the hybrid (designed for all regimes) and the linear controller (designed for linear regime only), are organized as:

- Varying vehicle velocity: tests done to check the adaptability of the system to uncertainties in vehicle velocity;
- Varying tire parameters: tests done to check the adaptability of the system to uncertainties in tire parameters;

Furthermore, the performance is examined in fault tolerance situations, i.e. during a system failure that makes only one of the actuators work: e.g. we demonstrate how the system can recover during braking system failure (ESP failure) when the only controllable actuator is steering, and how the system can recover during active steering system failure (AFS failure) when the only controllable actuator is braking. All simulations and comparisons are made without re-tuning the controller.

A. Performance with varying vehicle velocity.

The hybrid adaptive controller was tested at different vehicle velocities: 20 m/s (Figures 3 and 4) and 25 m/s (Figures 5 and 6)). It can be observed from Figure 3 that all three hybrid control algorithms limits the tracking error, even whenever there is switching to nonlinear handling regimes. Using a single linear controller as in Figure 4 gives poor performance leading the vehicle to spin. Therefore, having a hybrid adaptive controller seems of fundamental importance.
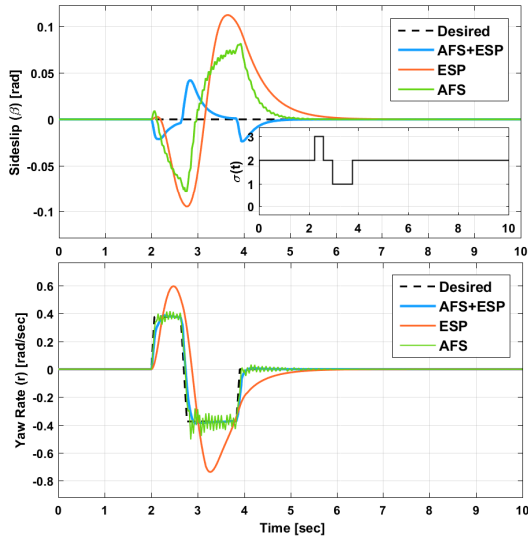
Fig. 7: Closed-loop response in SWD maneuver with hybrid adaptive control and low friction (in the small plot the switching signal is shown).

Fig. 8: Closed-loop response in SWD maneuver with linear controller and low friction.

TABLE II: Comparison: Maximum tracking error in yaw rate (r) with vehicle velocity of $20m/s$

Controller ⇒	Hybrid Adaptive		Linear	
Safety System ⇓	High Friction	Low Friction	High Friction	Low Friction
AFS	$1.29\cdot10^{-1}$	$1.43\cdot10^{-1}$	unstable	$2.58\cdot10^{-1}$
ESP	$2.58\cdot10^{-1}$	$4.99\cdot10^{-1}$	unstable	$6.43\cdot10^{-1}$
AFS + ESP	$7.54\cdot10^{-2}$	$8.40\cdot10^{-2}$	unstable	$2.56\cdot10^{-1}$

On the other hand, Figure 5 shows a stable system response even in the presence of uncertainty (in vehicle velocity), while a single linear controller again fails to handle the situation (Figure 6). The maximum tracking error is available in Table I from which it can be observed that it is smallest for the integrated control. Having the AFS only active leads to degradation in sideslip angle, while having the ESP only active leads to degradation in yaw rate.

TABLE I: Comparison: Maximum tracking error in yaw rate (r)

Controller ⇒	Hybrid Adaptive		Linear	
Safety System ⇓	20 m/s	25 m/s	20 m/s	25 m/s
AFS	$1.29\cdot10^{-1}$	$1.57\cdot10^{-1}$	unstable	unstable
ESP	$2.58\cdot10^{-1}$	$3.49\cdot10^{-1}$	unstable	unstable
AFS + ESP	$7.54\cdot10^{-2}$	$8.33\cdot10^{-2}$	unstable	unstable

B. Performance with varying tire parameters

The new tire parameters for these simulations are obtained by using soil instead of asphalt as in the previous case. The tire parameters used to carry out the simulations are available in Table IV in the Appendix. It is observed from Figure 7 that that errors are larger in view of the lower friction, but still all three control algorithms achieve the lateral stability of the vehicle when the hybrid adaptive control policy is adopted. Figure 8 shows that the linear control algorithm fails to generate enough yaw rate in order to follow the desired trajectory. The maximum tracking error is reported in Table II for the different situations.

V. CONCLUSIONS

The main contribution of this paper was to formulate an adaptive hybrid control strategy to achieve the lateral stability of a ve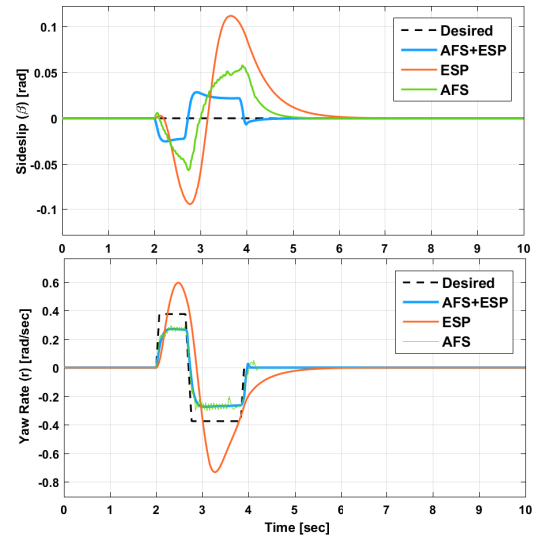hicle during difficult driving maneuvers and in the presence of uncertainty. The vehicle stability problem was formulated as an adaptive state tracking for a PWA system. A piecewise affine reference model was chosen to describe linear and nonlinear handling regimes. Significant performance improvement over linear control law was observed in all simulation results. Future work might be focusing on combining the proposed approach with friction estimation using multiple models [30], [31] or on coordinating in a more systematic way the vehicle safety subsystems using adaptive coordination [32], [33].

REFERENCES

[1] Y. Koh, H. Her, K. Kim and K. Yi, "Driver Model with Motion Stabilizer for Vehicle-Driver Closed-loop Simulation at High-speed Maneuvering ", *2015 IEEE Intelligent Vehicles Symposium (IV)*,p. 1299-1304, June 28 - July 1, 2015, COEX, Seoul, Korea.

[2] O. Gietelink, J. Ploeg, B. De Schutter, and M. Verhaegen, "Development of advanced driver assistance systems with vehicle hardware-in-the-loop simulations", *Vehicle System Dynamics*, vol. 44, no. 7, p. 569590, July 2006.

[3] P. Koopman and M. Wagner, "Challenges in Autonomous Vehicle Testing and Validation", *2016 SAE World Congress*, 2016.

[4] M. Nagai, M. Shino and F. Gao, "Study on Integrated Control of active front steer angle and direct yaw moment", *JSAE review*, vol. 23, no. 3, p. 309-315, 2002.

[5] S. S. You and S. K. Jeong, "Controller design and analysis of automatic steering of passenger cars", *Mechatronics*, vol. 12, no. 3, p. 427-446, 2002.

[6] D. Bernardini, S. Di Cairano, A. Bemporad and H.E. Tseng, "Drive-by-wire vehicle stabilization and yaw regulation: A hybrid model predictive control design", *Joint 48th IEEE Conference on Decision and Control and 28th Chinese Control Conference*, p. 7621-7626, Shanghai, P.R. China, Dec 16-18 2009.

[7] A. Benine-Neto and S. Mammar, "Piecewise Affine State Feedback Controller for Lane Departure Avoidance", *2011 IEEE Intelligent Vehicles Symposium (IV)*, p. 839-844, Baden-Baden, Germany, June 5-9, 2011.

[8] G. Palmieri, M. Baric, L. Glielmo, E. H. Tseng and F. Borrelli, "Robust Vehicle Lateral Stabilization via Set-Based Methods for Uncertain Piecewise Affine Systems: Experimental Results", *50th IEEE Conference on Decision and Control and European Control Conference (CDC-ECC)*, p. 3252-3257, Orlando, FL, USA, December 12-15, 2011.

[9] A. Benine-Neto and C. Grand, "Piecewise Affine Control for Fast Unmanned Ground Vehicles", *2012 IEEE/RSJ International Conference on Intelligent Robots and Systems*, p. 3673-3678, Vilamoura, Algarve, Portugal, October 7-12, 2012.

[10] L. Jianfeng and G. Li, "Neural Network Control Approach for Improving Vehicle Stability", *9th IEEE International Conference on Control, Automation, Robotics and Vision*, Singapore, 5-8 Dec, 2006.

[11] L. Li, H. Wang, J. Lian, X. Ding, and W. Cao, "A Lateral Control Method of Intelligent Vehicle Based on Fuzzy Neural Network", *Hindawi Publishing Corporation, Advances in Mechanical Engineering*, 20 September 2014.

[12] F. Tahami, S. Farhangi and R. Kazemi, "A fuzzy logic direct yaw-moment control system for all-wheel-drive electric vehicles", *Vehicle System Dynamics*, vol. 41, no. 3, p. 203-221, 2004.

[13] A. F. Idriz, A. S. Rachman, and S. Baldi, "Integration of Auto-Steering with Adaptive Cruise Control for Improved Cornering Behavior", *IET Intelligent Transport Systems*, accepted, scheduled for 2018.

[14] M. Di Bernardo, U. Montanaro and S. Santini, "Novel switched Model Reference Adaptive Control for continuous Piecewise Affine systems", *47th IEEE Conference on Decision and Control*, p. 1925-1930, 2008.

[15] M. Di Bernardo, U. Montanaro and S. Santini, "Minimal Control Synthesis Adaptive Control of Continuous Bimodal Piecewise Affine System", *SIAM Journal on Control and Optimization*, vol. 48, no. 7, p. 4242-4261, 2010.

[16] M. Di Bernardo, U. Montanaro and S. Santini, "Hybrid Model Reference Adaptive Control of Piecewise Affine Systems", *IEEE Transactions on Automatic Control*, vol. 58, no. 2, p. 304-316, 2013.

[17] M. Di Bernardo, U. Montanaro, R. Ortega and S. Santini, "Extended Hybrid Model Reference Adaptive Control of Piecewise Affine Systems", *Nonlinear Analysis: Hybrid Systems*, vol. 21, p. 11-21, 2016.

[18] Q. Sang and G. Tao, "Adaptive control of piecewise linear systems: the state tracking case", *IEEE Transactions on Automatic Control*, 57(2):522 528, 2012.

[19] S. Yuan, B. De Schutter and S. Baldi, "Adaptive asymptotic tracking control of uncertain time-driven switched linear systems", *IEEE Transactions on Automatic Control*, vol. 62, no. 11, p. 5802-5807, 2017.

[20] R. Rajamani, *Vehicle Dynamics and Control*, Springer, second edition, 2012.

[21] A. Benine-Neto, S. Scalzi, M. Netto, S. Mammar and W. P. Lepine, "Vehicle Yaw Rate Control based on Piecewise-Affine Regions", *2010 IEEE Intelligent Vehicle Symposium*, p. 20-25, University of California, San Diego, CA, USA, June 21-24 2010.

[22] S. Sadri and C. Wu, "Stability analysis of a nonlinear vehicle model in plane motion using the concept of Lyapunov exponents", *Vehicle System Dynamics - International Journal of Vehicle Mechanics and Mobility*, vol. 51, no. 6, p. 906-924, 2013.

[23] H. B. Pacejka, *Tyre and Vehicle Dynamics*, Butterworth-Heinemann, 2012.

[24] Q. Sang and G. Tao, "Multivariable Adaptive Piecewise Linear Control Design for NASA Generic Transport Model", *Journal of Guidance, Control, and Dynamics*, vol. 35, no. 5, p. 1559-1567, 2012.

[25] S. Yuan, B. De Schutter and S. Baldi, "Robust adaptive tracking control of uncertain slowly switched linear systems", *Nonlinear Analysis: Hybrid Systems*, vol. 27, p. 1-12, 2018.

[26] J. P. Hespanha, and A. S. Morse, "Stability of Switched Systems with Average Dwell Time", *Proceedings of the IEEE Conference on Decision and Control*, p. 2655 - 2660, Phoenix, Arizona, USA, 1999.

[27] D. Liberzon and A. S. Morse, "Basic Problem in Stability and Design of Switched System", *IEEE Control Systems*, vol. 19, no. 5, p. 59-70, 1999.

[28] D. Liberzon, *Switching in Systems and Control*, Springer Science & Business Media, Birkhauser, Boston, 2003.

[29] G. Tao, *Adaptive control design and analysis*, John Wiley & Sons, 2003.

[30] D. Ghosh, *Optimal Model Distribution in Adaptive Switching Control*, Master's Thesis, Delft University of Technology, Delft, The Netherlands, 2015.

[31] D. Ghosh and S. Baldi, "Optimal Model Distributions in Supervisory Adaptive Control", *IET Control Theory and Applications*, vol. 11, no. 9, p. 13801387, 2017.

[32] M. Romagnuolo, *Estimating uncertainties in cooperative networks*, Master's Thesis, Delft University of Technology, Delft, The Netherlands, 2018.

[33] I. Michailidis, S. Baldi, E. B. Kosmatopoulos, and P. A. Ioannou, "Adaptive Optimal Control for Large-Scale Nonlinear Systems", *IEEE Transactions on Automatic Control*, vol. 62, no. 11, p. 5567-5577, 2017.

APPENDIX

TABLE III: Vehicle model parameters

	Description	Value	Unit
$\hat{\alpha}_f$	saturation limit	0.101	rad
c_f	front tire cornering stiffness	$9.059 * 10^4$	N/rad
d_f	front tire PWA coefficient	$-9.059 * 10^3$	N/rad
e_f	front tire PWA coefficient	$1.005 * 10^4$	N/rad
c_r	rear tire cornering stiffness	$1.651 * 10^5$	N/rad
d_r	rear tire PWA coefficient	$1.651 * 10^5$	N/rad
e_r	rear tire PWA coefficient	0	N/rad
l_f	distance of COG from front axle	1.47	m
l_r	distance of COG from rear axle	1.43	m
m	mass of vehicle	1891	kg
I_z	yaw moment of inertia	3213	kgm^2
v_x	longitudinal velocity	20	m/s
λ	longitudinal slip	0	

TABLE IV: Vehicle tire parameters with low friction

	Description	Value	Unit
$\hat{\alpha}_f$	saturation limit	0.07	rad
c_f	front tire cornering stiffness	$3.999 * 10^4$	N/rad
d_f	front tire PWA coefficient	$-1.116 * 10^4$	N/rad
e_f	front tire PWA coefficient	$2.018 * 10^3$	N/rad
c_r	rear tire cornering stiffness	$3.499 * 10^4$	N/rad
d_r	rear tire PWA coefficient	$3.499 * 10^4$	N/rad
e_r	rear tire PWA coefficient	0	N/rad